



# Boosting Fenton-like reaction efficiency by co-construction of the adsorption and reactive sites on N/O co-doped carbon

Sijin Zuo<sup>a</sup>, Shengcai Zhu<sup>b</sup>, Jiaying Wang<sup>a</sup>, Weiping Liu<sup>a</sup>, Juan Wang<sup>a,\*</sup>

<sup>a</sup> Institute of Environmental Health, College of Environmental & Resource Sciences, Zhejiang University, Hangzhou 310058, China

<sup>b</sup> School of Materials, Sun Yat-Sen University, Guangzhou 510275, China

## ARTICLE INFO

### Keywords:

Metal-free catalyst  
Reaction site  
Water remediation  
Singlet oxygen  
Wide pH range

## ABSTRACT

A N/O-codoped carbon-based catalyst (N/O-C-8) designed with dual reaction sites (pyridinic N and carbonyl group) was fabricated in this work, for persulfate based advanced oxidation reaction. The pyridinic N served as the adsorption site for target molecule, via series of high resolution XPS analysis and DFT calculation. Meanwhile, the carbonyl group functioned as the persulfate activation site, to generate oxidative <sup>1</sup>O<sub>2</sub>. Engineering and isolating the two reaction sites on catalyst surface can greatly shorten the migration distance from <sup>1</sup>O<sub>2</sub> to target organic molecule, resulting in good catalytic removal efficiency. As demonstrated, during a 4-hour continuous flow experiment, our catalyst showed stable and efficient removal of tetracycline, with a flow rate of 4 mL/min. The study provides keen insights into the design of effective non-metal based catalysts for practical water remediation.

## 1. Introduction

The active radical ( $\bullet\text{OH}$  and  $\text{SO}_4^{\bullet-}$ ) - based advanced oxidation processes (AOPs) have shown their promising potential in the environmental treatment of organic pollutants, since the active radicals own high redox potentials (e.g. 1.8–2.7  $V_{\text{NHE}}$  for  $\bullet\text{OH}$ , 2.5–3.1  $V_{\text{NHE}}$  for  $\text{SO}_4^{\bullet-}$ ), and can easily oxidize the organic molecule with high universality [1–5]. Hydrogen dioxide ( $\text{H}_2\text{O}_2$ ) based AOPs have shown their efficiencies for organic pollutant decontamination, however, they always suffer from the restricted pH working range (normally  $\sim 3$ ), and issues for the storage and transport of the liquid  $\text{H}_2\text{O}_2$  [6]. The emergence of persulfate based AOPs recently received great attention since the solid persulfate is more convenient and shows broader pH adaptation [7]. Various heterogeneous catalysts were fabricated for the reactions, including  $\text{Fe}_2\text{O}_3$  @Zn/Co-ZIF [8], 1T-2H  $\text{MoS}_2$  [9], nanodiamond [10–12] and etc [13–17]. In comparison with metal-based composites, metal-free carbon based catalysts not only can avoid metal leaching to cause second contamination of water resources, but also present cost-effective strategies due to the use of earth-abundant elements [18–21]. Construction of metal-free catalysts with high catalytic performance owns great potential for the practical wastewater treatment.

Typically, in the persulfate based heterogeneous advanced oxidation reactions, the process can be mainly divided into three main steps. First,

the activation of persulfate to produce active species (e.g.  $\bullet\text{OH}$  and  $\text{SO}_4^{\bullet-}$ ). Second, the migration of active species to reach the target molecule. Third, the oxidation of the target molecule by the active species. Since lifetime of the active species are normally quite short (1  $\mu\text{s}$  for  $\bullet\text{OH}$ , for example) [22,23], adsorption of target molecule on catalyst surface can reduce the migration distance of active species to the target molecule, boosting the oxidation degradation efficiency [24–26]. For example, biochars [24], reduced graphene oxide [27,28] and porous carbon [26,29] have been reported as efficient catalysts for organic pollutant removal, with remarkable adsorption capability to organic contaminants. However, the non-site-directed adsorption of target molecule on catalyst surface may spatially block the reaction sites for persulfate activation, restraining the generation of active species and finally the overall removal efficiency [30,31]. Therefore, strategies to construct dual reaction sites on metal-free catalyst to co-locate but separate the organic compound adsorption and persulfate activation are highly demandable.

Here in this work, we fabricated a N/O-codoped carbon based composite for the efficient removal of tetracycline through activation of peroxydisulfate (PDS). Annealing temperature of the composite was tuned to regulate the N and O contents, and the optimized N/O-C-8 composite owns a high doping amount of N and O (10.04 wt% and 7.30 wt%, respectively). Through a series of high resolution XPS analysis

\* Corresponding author.

E-mail address: [wjuan@zju.edu.cn](mailto:wjuan@zju.edu.cn) (J. Wang).

<https://doi.org/10.1016/j.apcatb.2021.120783>

Received 24 August 2021; Received in revised form 23 September 2021; Accepted 29 September 2021

Available online 2 October 2021

0926-3373/© 2021 Elsevier B.V. All rights reserved.

and density functional theory (DFT) calculations, we demonstrated that the pyridinic N and carbonyl group on the catalyst surface served as the adsorption site for target organic molecule tetracycline and reaction site for PDS, respectively. In the degradation experiment, the catalyst N/O-C-8 shows a fast removal of tetracycline with  $k$  value of  $1.50\text{ min}^{-1}$ , which is by far the highest rate for advanced oxidative removal of tetracycline. A lab-scale continuous flow experiment revealed that the N/O-C-8/PDS system can efficiently degrade tetracycline continuously for  $\sim 5\text{ h}$ . Moreover, this catalyst also presents high removal efficiency towards other organic pollutants such as rhodamine B, bisphenol A and 2,4-dichlorophenol. Additionally, this system shows stable efficiency in the presence of widely detected natural organic matter and anions (such as humic acid,  $\text{Cl}^-$ ,  $\text{F}^-$  and  $\text{NO}_3^-$ ), with a broad pH working range (2–9). In this case, our study unveils a design strategy of non-metal carbon based catalyst for efficient and stable remediation of the organic contaminants for potential practical use.

## 2. Materials and methods

### 2.1. Chemicals

Tetracycline hydrochloride (98.0%), dicyandiamide (DCD, 99.8 wt %), 2,4-dichlorophenol and ethylene diamine tetraacetic acid (EDTA, 99.5%) were purchased from J&K Co Ltd. Concentrated sulfuric acid ( $\text{H}_2\text{SO}_4$ , 98%), sodium hydroxide (NaOH, 97.0%), sodium chloride (99.5%), sodium nitrate ( $\geq 99.0\%$ ) and potassium bicarbonate (99.9%) were obtained from Sinopharm Chemical reagent Co., Ltd. Glutaraldehyde (analytical reagent, 50% in  $\text{H}_2\text{O}$ ), bisphenol A, 5,5-dimethyl-1-pyrrolidine N-oxide (DMPO, 97%), 2,2,6,6-tetramethyl-4-piperidinol (TEMP, 98.0%) and  $\text{K}_2\text{S}_2\text{O}_8$  (99.0%) were supplied by Aladdin Chemical Co., Ltd. L-histidine (98.5%), humic acid (90.0%), potassium fluoride (99.0%), sodium nitrate (98.5%), benzoic acid (99.0%), methanol (HPLC grade), rhodamine B (AR grade) and formic acid (HPLC grade) were purchased from Macklin Chemical Co., Ltd. Ketjen black was obtained from Lion Co., Ltd. All chemicals were used directly if without additional notification. Deionized (DI) water was produced by Millipore Mili-Q IQ 7000.

### 2.2. Synthesis of the catalyst composites

The nitrogen/oxygen co-doped carbon materials (N/O-C-X, X denoted the annealing temperature) were prepared by the following procedures. 60 mg ketjen black as main carbon source was mixed with 5 mL DI water under ultrasonication. After that, 7 mmol EDTA, and 0.13 mol DCD were subsequently added and mixed well with the mixture, with the assistance of ultrasonication and ball milling. After that, the as-prepared mixture was pyrolyzed at  $650\text{--}900\text{ }^\circ\text{C}$  under argon gas protection. The obtained black powder was collected and washed with DI water for three times. Finally, washed powder was dried at  $80\text{ }^\circ\text{C}$  and stored for further experiments.

### 2.3. Catalytic experiment

The degradation experiments were carried out in a 50 mL glass beaker under magnetic stirring at ambient temperature. Typically, 2 mg catalyst was added into the reactor beaker which containing 20 mL tetracycline aqueous solution (10 mg/L). The mixture was stirred for 30 min at ambient temperature to establish adsorption-desorption equilibrium. After that, the experiment was triggered by adding 1 mg PDS into the solution. During the degradation experiment, at regular time intervals, certain amount of the mixture solution was fetched from the reactor and was added with 0.2 mL L-histidine (0.2 M) immediately to terminate the reaction. The mixture solution was then filtered with a  $0.22\text{ }\mu\text{m}$  PTFE filter and the collected solution was sent for HPLC analysis, detailed detection parameters were presented in the [supporting information](#).

### 2.4. Characterization

Morphologies of the composites were observed by transmission electron microscope (JEM 1200) at 120 kV, high-resolution transmission electron microscope (HRTEM, FEI Tecnai F20) at 200 kV and field emission scanning electron microscope (FE-SEM, Gemini SEM 300, SE2). Electron energy loss spectroscopy (EELS) was acquired by a FEI Titan ChemiSTEM with a probe aberration corrector and super EDX, which is conducted at 200 kV. X-ray diffraction patterns were carried out on a powder X-ray diffractometer (Bruker D8 Advance) equipped with  $\text{Cu K}\alpha$  radiation ( $\lambda = 1.5406\text{ \AA}$ ). X-ray photoelectron spectroscopy (XPS) was measured by K-alpha X-ray photoelectron spectrometer (Thermo Fisher Scientific, USA). The special surface area of catalyst was analyzed by a surface area and porosity analyser (TriStar II 3020, Micromeritics, Norcross, GA) based on the method of Brunauer-Emmett-Teller (BET). Electron paramagnetic resonance (EPR) spectra were performed by an EMX-10/12, Bruker, Germany. Raman spectra were measured with a solid-state laser (wavelength at 532 nm) micro-Raman spectrometer (LabRAM, Horiba Jobin Yvon). Photoluminescence emission spectra was collected by a Jasco spectrophotometer under 270 nm excitation. UV–visible absorption spectrum was acquired from an Agilent UV–vis spectrophotometer (Cary-5000). Metal ions were measured by the Inductively Coupled Plasma Mass Spectrometry (ICP-MS, Agilent Technologies 7800 ICP-MS). Concentrations of inorganic ions were detected by the Ion Chromatography (IC, DIONEX AQUION). Total organic carbon (TOC) measurement was performed by a TOC analyser (JENA, MULTI N/C 3100, Germany).

### 2.5. Computational framework

The adsorption energy calculation was performed using the plane wave density functional theory program, Vienna ab initio simulation package (VASP) where the electron-ion interactions of C, O, and N atoms were represented by the projector augmented wave scheme. The exchange-correlation functional was described by the generalized gradient approximation (GGA) in the Perdew-Burke-Ernzerhof (PBE) parameterization. We use big cell with size of  $14 \times 17 \times 15\text{ \AA}$  for surface model. The calculations were performed using a modest  $1 \times 1 \times 1$   $k$ -point grid set generated by the Monkhorst-Pack scheme, which was tested accurate enough for the present system. The energy cutoff was 450 eV. In order to account for the van der Waals (vdW) interaction, we incorporated dispersion corrections using the optPBE functional.

## 3. Results and discussion

### 3.1. Fabrication and structure analysis of the N/O-C-X series

The schematic diagram for the fabrication of N/O-C-8 composite was shown in Fig. 1a. Typically, ethylene diamine tetraacetic acid (EDTA) and dicyandiamide (DCD) were mixed well with ketjen black. The mixture was pyrolyzed at  $800\text{ }^\circ\text{C}$  [32]. The weight change during the pyrolysis process was analyzed via TGA (Fig. S1). Here, EDTA and DCD were selected and manifested as the oxygen and nitrogen source, respectively (Fig. S2). Structure analysis to the composite was first performed via XRD analysis. The diffraction peaks at around  $26^\circ$  and  $43^\circ$  in the XRD spectrum corresponded to the (002) and (100) planes of the graphitic structure (Fig. 1b) [33,34]. The selected-area electron diffraction (SAED) inserted in Fig. 1c indicated the amorphous pattern of the composite, matching well with the XRD result. The high-resolution transmission electron microscopy (HRTEM, Fig. 1d) and scanning electron microscopy images (Fig. 1e) revealed the porous structure of the synthesized N/O-C-8 composite. Meanwhile, the element mapping images (Fig. 1f-h) showed the uniform distribution of C, N and O elements inside the composite, respectively. The X-ray photoelectron spectroscopy (XPS) survey spectrum of N/O-C-8 revealed the only existence of N, O and C elements in N/O-C-8, matching with the electron diffraction

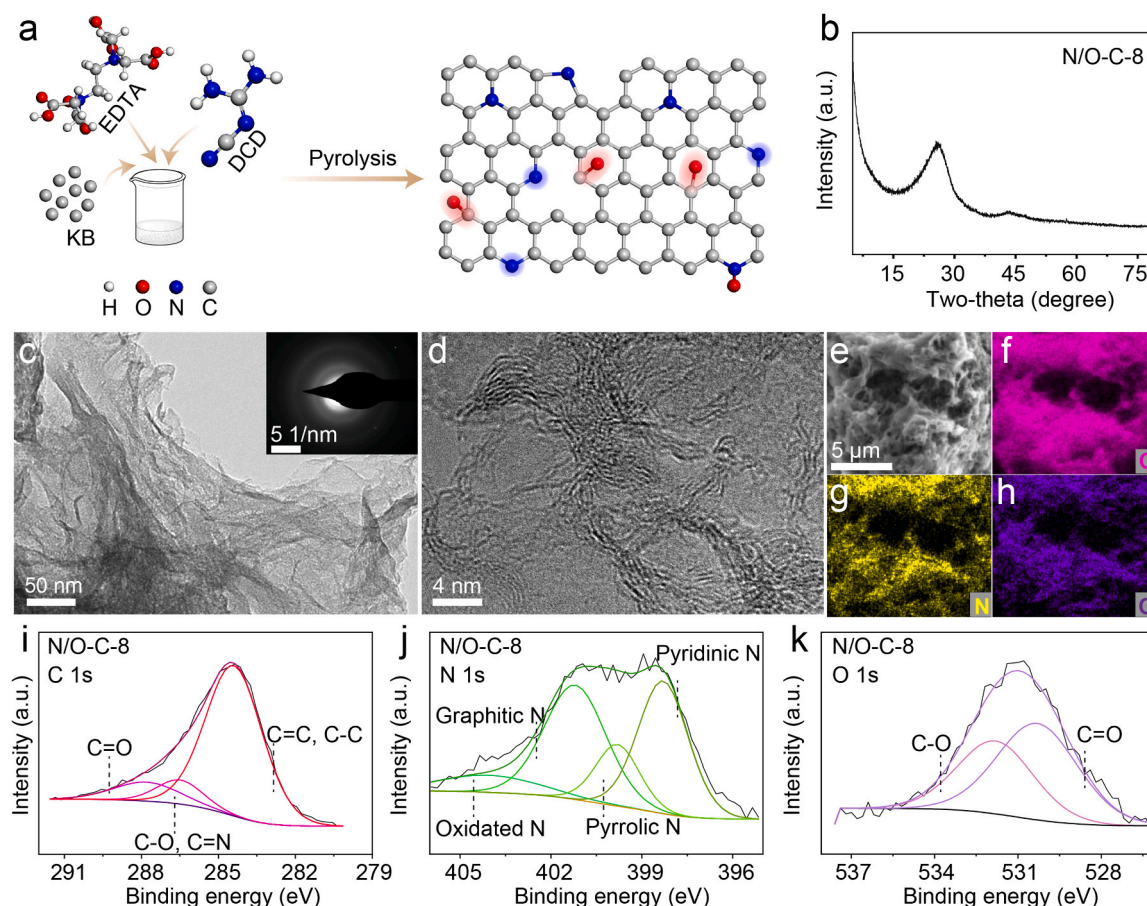


**Fig. 1.** The preparation and characterization of N/O-C-8. a) Schematic illustration for the synthesis of N/O-C-X composite. b) The X-ray diffraction pattern of the prepared N/O-C-8 composite. c) and d) The low and high resolution TEM images of N/O-C-8. e) The SEM images of N/O-C-8. e-f) The corresponding elemental mapping images of N/O-C-8 presented in e. i-k) The respective C 1s, N 1s and O 1s high resolution XPS spectra analysis of N/O-C-8.

results above. The high resolution XPS analysis unveiled the respective element configurations in N/O-C-8 (Fig. 1i-k).

Effect of pyrolysis temperature on the composite was investigated via annealing the mixture at different temperatures to form N/O-C-X ( $X = 6.5, 7-9$ , which represents the temperature, e.g. 6.5 represents 650 °C). As indicated by the XRD spectra, low-resolution TEM images and BET results (Fig. S3-S5), high temperature can produce large surface area and generate more pores in the composite, which may be contributed by the increased interlamellar space and release of gas during the thermal expansion process [35]. However, the defect degree of N/O-C-X increased first with the temperature (from 650 °C to 750 °C) and decreased subsequently from 750 °C to 900 °C (Fig. S6 and S7). The increased defects at the beginning may be caused by the thermal expansion process, while a further increased temperature would result in the releasing of N and O, as well as their rearrangement to achieve low energy structure [36]. To verify this, XPS survey and high resolution spectra analysis were performed to the composites. The XPS survey spectra (Fig. S8) only showed the presence of C, N and O elements, similar to N/O-C-8. However, the content of N in composites N/O-C-X ( $X = 6.5-9$ ) decreased with the elevated temperature (Table S1), and meanwhile the graphitic N content increased gradually (Fig. S9 and Table S2), matching with the defect analysis above.

### 3.2. Catalytic performance analysis of the N/O-C-X series

The catalytic performance of N/O-C-X series were analyzed via activating PDS for removal of organic contaminant. Tetracycline, as one of the widely detected antibiotic contaminants [37], was chosen as the

target compound. Amount of PDS and catalyst involved in the reaction was optimized, respectively (Fig. S10). As shown in Fig. 2a, the catalytic performance of N/O-C-X series increased with the elevated pyrolysis temperature, and reached the highest rate when the catalyst was pyrolyzed at 800–900 °C (N/O-C-8/9). The pseudo-first order reaction kinetic constant ( $k$  value) of N/O-C-9 and N/O-C-8 was both  $1.5 \text{ min}^{-1}$  which is 9.6-fold and 11.9-fold higher than N/O-C-7 and N/O-C-7.5, respectively. In comparison with literatures, N/O-C-8 presented an excellent removal performance (Table S3). As mentioned above, the defect degrees of N/O-C-8/9 are both smaller than N/O-7.5, therefore the defects may not determine the removal efficiency dominantly.

To deep investigate the removal performance of the N/O-C-X series, we analysed their adsorption capability toward tetracycline firstly. As shown in Fig. 2c, the composites showed a gradually increased adsorption capability toward tetracycline from  $X = 6.5-9$ . We fitted their adsorption efficiencies with the total removal rates linearly (Fig. S11b). The relatively low  $R^2$  value of 0.80 indicated that the adsorption may contribute but not the only dominant factor. The degradation of tetracycline by the active species generated from PDS may also play the key role. In a further experiment, we measured the change of PDS concentration under presence of the respective catalysts to investigate their PDS activation performance. As can be seen (Figs. 2b, S12), from N/O-C-6.5 to N/O-C-9, the activation of PDS ( $k_{\text{PDS}}$ ) is in an overall increasing trend, similar with the total removal efficiency of tetracycline. The existence of tetracycline during the reaction using N/O-C-8 catalyst was monitored via HPLC. As can be seen (Fig. 2c), the tetracycline is not detectable at reaction time of 10 min. It should be mentioned that, after the reaction, we collected the catalysts and washed

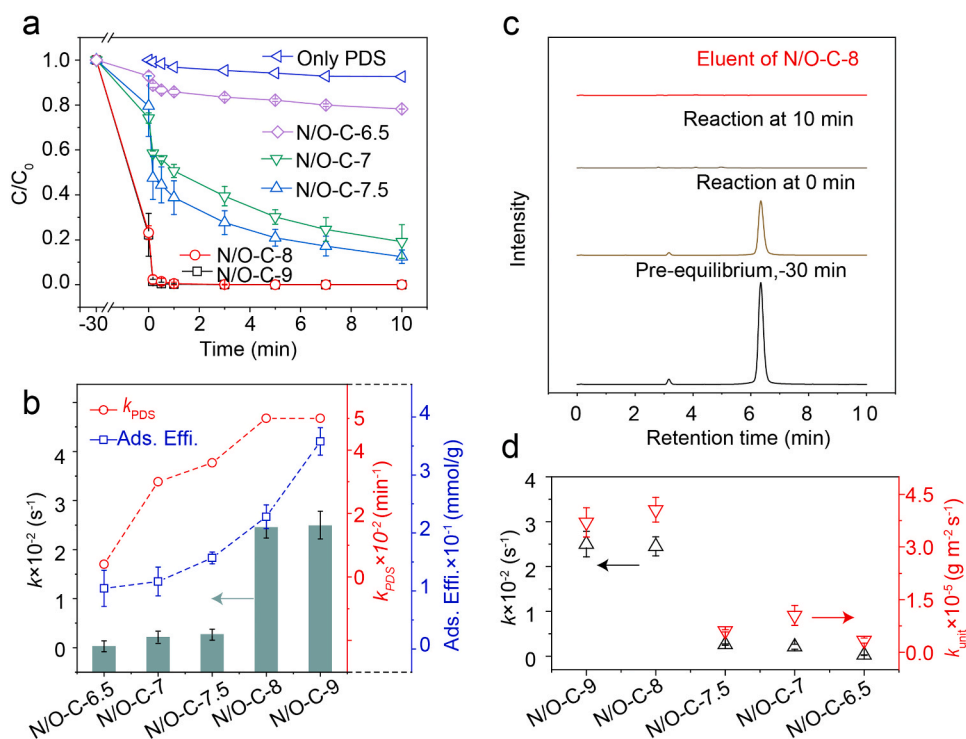


**Fig. 2.** The catalytic performance analysis of N/O-C-X series. a) The degradation curves of tetracycline with N/O-C-X (X = 6.5–9) PDS and only PDS system, respectively. b) The comparison of  $k$  value,  $k_{PDS}$  and adsorption efficiency for N/O-C-X composites. c) Determination of tetracycline during the reaction process via HPLC analysis. d) The  $k$  value of N/O-C-X series and the corresponding reaction rate normalized with surface areas ( $k_{unit}$ ). Reaction condition: [tetracycline] = 10 mg/L, [PDS] = 0.18 mM, [catalyst] = 0.1 g/L, reaction volume = 20 mL, pre-equilibrium 30 min before reaction.

with methanol for several times [38]. The non-detectable tetracycline in the eluent suggests that the adsorbed organic compound was completely degraded. Therefore, we propose that an adsorption assisted catalytic degradation of tetracycline dominates the overall removal of

tetracycline. Additionally, as surface area was widely reported to determine the adsorption efficiency and the surface area of the composites varied a lot (Fig. S5) [25,39,40], we calculated the removal rate of tetracycline per  $m^2$  surface area, of the respective catalyst, to

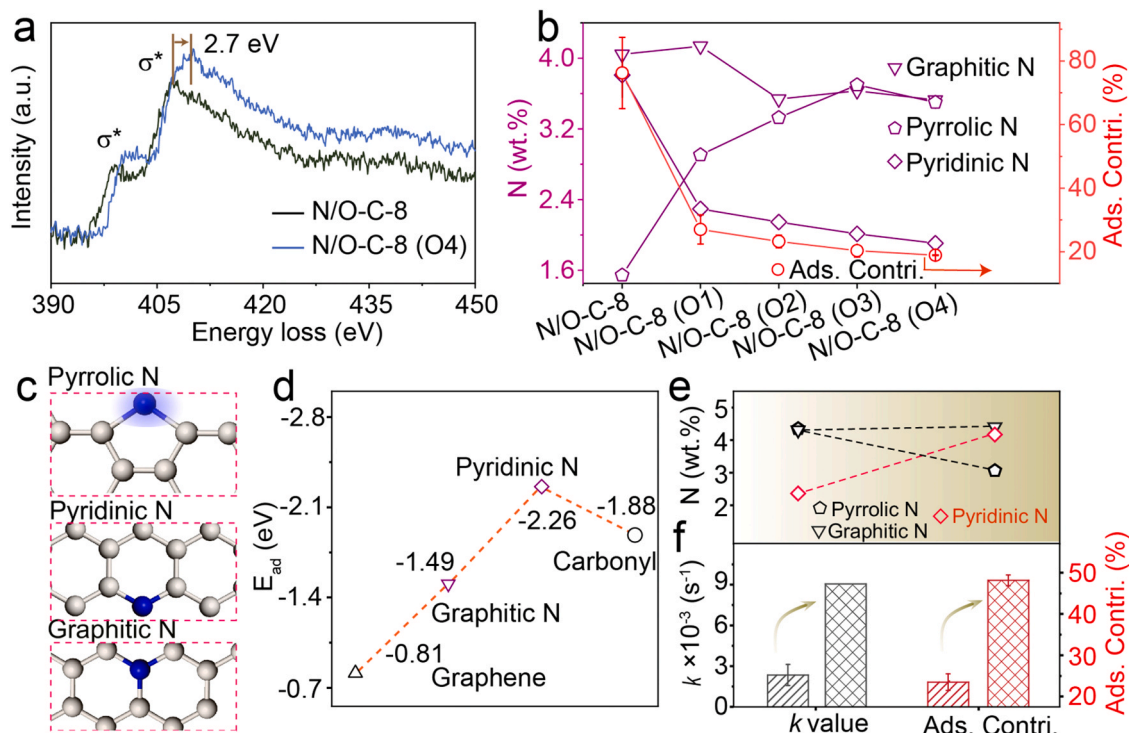


**Fig. 3.** Identification of the active sites for the adsorption capability. a) Nitrogen K-edge EELS spectra of N/O-C-8 and N/O-C-8 (O4). b) The plotted adsorption contribution, content of pyridinic N, pyrrolic N and graphitic N for oxidized N/O-C-8 series. c) The schematic illustration of pyridinic N, pyrrolic N and graphitic N, respectively. d) The calculated adsorption energy of different sites on catalyst surface towards tetracycline. e) Analysis of different nitrogen contents before and after compensatory of nitrogen. f) The  $k$  values and adsorption contributions of N/O-C-8 (O3) before and after compensatory of nitrogen. Reaction condition: [tetracycline] = 10 mg/L, [PDS] = 0.18 mM, [catalyst] = 0.1 g/L, reaction volume = 20 mL, pre-equilibrium 30 min before reaction.

investigate the influence of surface area on the removal efficiency. As can be seen (Fig. 2d), although both N/O-C-8 and 9 presented the similar overall removal efficiency, the calculated  $k$  value per  $\text{m}^2$  surface area ( $k_{\text{unit}}$ ) of N/O-C-8 is higher than N/O-C-9, indicating that the reaction sites on the composites are different and the reaction sites are mainly responsible for the reaction.

### 3.3. Exploration of the dual reaction site catalytic mechanism

Exploration of the main sites on the catalyst responsible for the reaction was performed. We choose N/O-C-8 as the representative sample since it shows the best removal performance. We oxidized N/O-C-8 with different amount of oxidants, respectively (see supporting information for detailed experiment). The treated N/O-C-8 samples are named as N/O-C-8 (O1-O4), in accordance to the increased oxidant amount used. Electron energy loss spectroscopy (EELS) analysis was conducted to N/O-C-8 and N/O-C-8 (O4) to investigate the change on the configuration of the N, O and C elements. As shown in Fig. 3a, a positive shift around 2.7 eV occurs to the N K-edge EELS spectra, while the spectra of C and O remain almost unchanged (Fig. S13), indicating that oxidation of N/O-C-8 changed the nitrogen configuration significantly [41].

The high resolution N 1 s XPS analysis was carried out to the oxidized N/O-C-8 composites and different N type contents (N wt%) were calculated accordingly. The N contents were calculated based on the element mass ratio and the corresponding high resolution XPS peak area. As presented in Fig. 3b and S14a, the pyridinic N content decreased gradually from N/O-C-8 to N/O-C-8 (O4), while pyrrolic N content increased and ratio of graphitic N remained relatively constant. The oxidation treatment didn't bring any significant change to the functional carbonyl groups (Fig. S14b and Table S4), which matched well with the EELS analysis above. The oxidized N/O-C-8 composites were applied for the Fenton-like removal of tetracycline (Fig. S15). N/O-C-8 (O1) presented much reduced adsorption efficiency and the adsorption contribution continuously decreased from N/O-C-8 (O2) to N/O-C-8 (O4). The  $k$  value of N/O-C-8 (O1-O4) series for tetracycline removal show same trend with the adsorption contribution (Fig. S16), which suggest that oxidation of the catalysts may mainly affect the adsorption capability. It can be seen that (Fig. 3b), only the pyridinic N content shows the similar trend with the adsorption capability. This phenomenon suggests that pyridinic N may be responsible for the adsorption. The adsorption energies ( $E_{\text{ad}}$ ) of different N to tetracycline were calculated via DFT

computation (Figs. 3c, d and S17). Pyridinic N shows the highest  $E_{\text{ad}}$ , unveiling its favorable adsorption capability towards tetracycline. To further confirm the role of pyridinic N, we annealed N/O-C-8 (O3) under ammonia gas atmosphere at 500 °C to compensate the N content [42]. Via high resolution N 1 s XPS analysis, it can be seen that, more pyridinic N were generated on the composite (Figs. 3e and S18a), with boosted adsorption contribution and removal efficiency of tetracycline (Figs. 3f and S18b). Based on the above investigations, it is clearly demonstrated that pyridinic N on the catalyst serves as the main adsorption site for target molecule tetracycline.

As we analyzed above, activation of PDS played the key role for the catalytic degradation of tetracycline. As shown in Fig. 4a, the concentration of PDS decreased with the similar ratio around  $0.05 \text{ min}^{-1}$ , under the existence of N/O-C-8 to N/O-C-8 (O4), indicating a stable PDS activation rate. The stable PDS activation suggests that the reaction site for PDS activation exists stably on the catalyst. Through the high-resolution analysis of the N and O 1 s XPS spectra (Fig. S14b and Table S4), we can see that, content of carbonyl group remains unchanged in the oxidized catalysts. This result suggests that the carbonyl group may function as the activation site for PDS. To further verify this, the glutaraldehyde modification technique was adopted to bring more carbonyl groups to catalyst N/O-C-7.5 [43]. As can be seen (Figs. 4b and S19a), after the modification of N/O-C-7.5 with glutaraldehyde, the carbonyl group amount on N/O-C-7.5 increased, as well as the corresponding PDS activation rate (Fig. 4c) and the overall tetracycline removal efficiency (Fig. 4d and S19b). It should be pointed out that, the replenishing of carbonyl group didn't contribute to the adsorption capability (Fig. 4e), which further proves that the improved removal efficiency of tetracycline in this system is mainly ascribed to the enhanced activation of PDS. The slightly decreased adsorption contribution may be possibly due to the steric blocking of the adsorption sites by the glutaraldehyde. Additionally, the tetracycline removal performance of N/O-C-X series also show a positive relationship with their carbonyl group they contained (Fig. S20). Via the above sets of experiments, it can be elucidated that the carbonyl group be mainly responsible for the activation of PDS.

As we mentioned above, the raw materials DCD and EDTA serve as the respective nitrogen and oxygen sources. To further validate the roles of pyridinic N and carbonyl group for the reaction, amount of DCD and EDTA adopted for the catalyst synthesis was tuned and the as-synthesized composites were analyzed, respectively (Figs. 5 and S21).

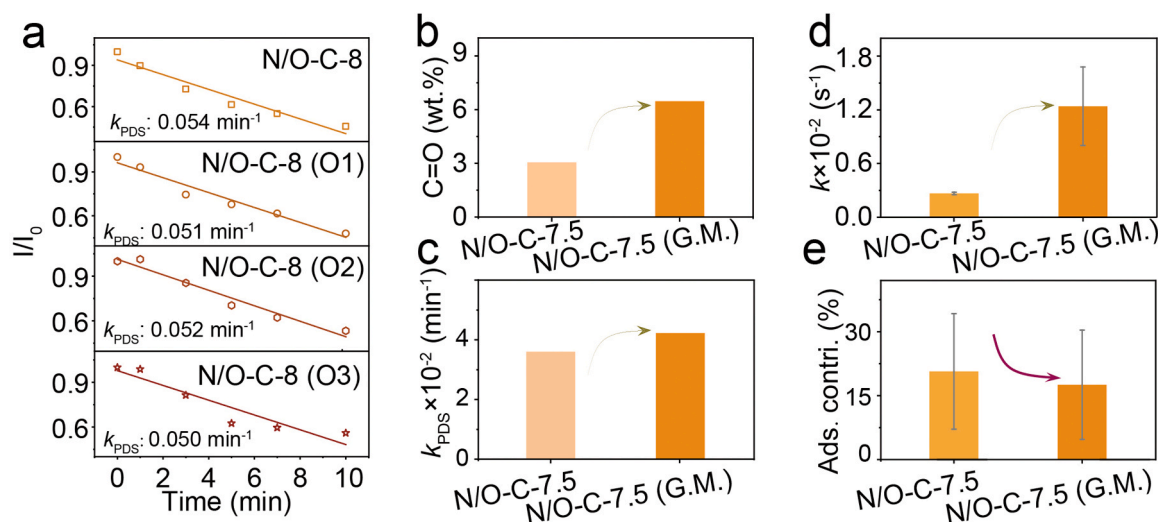


**Fig. 4.** Identification of the reaction site for PDS activation. a) The calculated activation rate of PDS ( $k_{\text{PDS}}$ ) under the oxidized N/O-C-8 series. Reaction condition: [catalysts] = 0.1 g/L, [tetracycline] = 0 mg/L, [PDS] = 0.18 mM, reaction volume = 20 mL. Note that the calculation was based on the detection of PDS concentration by potassium iodide colorimetric method. b-e) The comparison of the catalyst N/O-C-7.5 before and after glutaraldehyde modification (N/O-C-7.5 (G. M.)) through b) the content of carbonyl group, c)  $k_{\text{PDS}}$  value, d)  $k$  value for removal of tetracycline and e) adsorption efficiency of tetracycline, respectively.

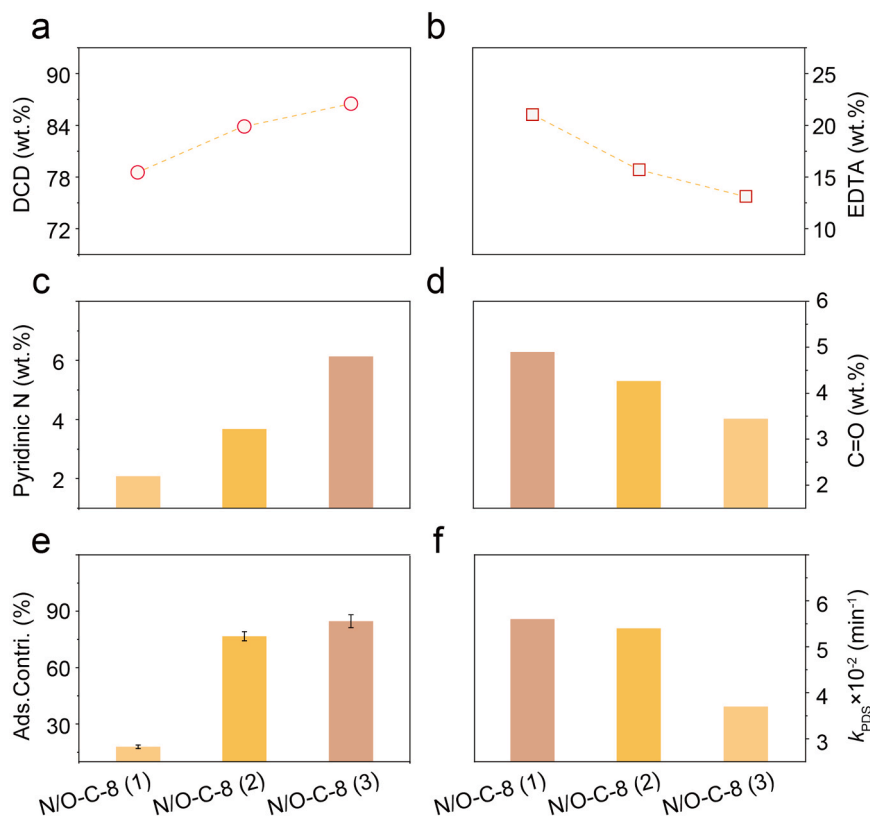
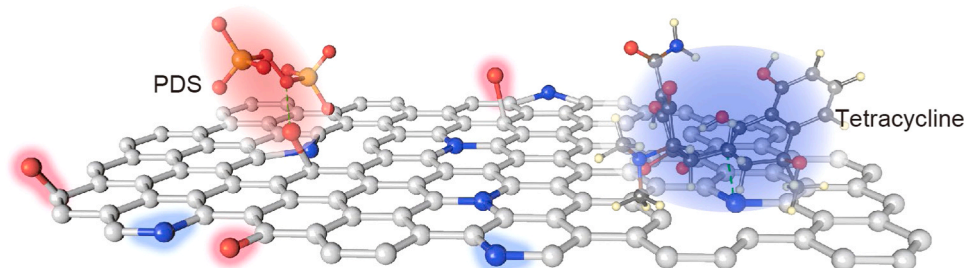


**Fig. 5.** Investigation of the reaction sites on the catalyst series. a and b) The tuning of DCD and EDTA amount, respectively. c and d) The change of pyridinic N and C=O group content, respectively. e and f) The value of adsorption contribution and  $k_{PDS}$  for N/O-C-8 (1–3), respectively. Reaction condition if required: [catalyst] = 0.1 g/L, [tetracycline] = 10 mg/L, [PDS] = 0.18 mM, reaction volume = 20 mL.

Composite N/O-C-8 (1–3) refer to the composite prepared with same condition as N/O-C-8, except the varied DCD and EDTA amount ratio (please refer to [supporting information](#) for the detailed sample preparation). As can be seen (Fig. 5a and c), increased DCD content can bring more pyridinic N, and the resulted composite showed higher adsorption capability (Fig. 5e). While in contrast, with reduced EDTA amount ratio, the carbonyl group amount in composite N/O-C-8 (1–3) decreased, as well as the the PDS activation rate (Fig. 5b, d and f). Based on above investigations, we can propose that dual reaction sites exist simultaneously on our catalysts, as displayed in Scheme 1. The pyridinic N serves as the adsorption site for tetracycline, while the carbonyl group helps to activate PDS. Once the PDS was activated, the active species generated from PDS will migrate to reach and react with the adsorbed tetracycline.

### 3.4. Identification of the involved active species and investigation of the practical application

EPR technique was applied to detect the active species involved in the system via using DMPO as the trapping agent firstly. The absence of signals for DMPO- $\bullet\text{OH}$  and DMPO- $\text{SO}_4^{\bullet-}$  adduct revealed that  $\bullet\text{OH}$  and  $\text{SO}_4^{\bullet-}$  radicals were not involved in the reaction (Fig. 6a) [44]. The presented peaks of the strong oxydic 5,5-dimethylpyrrolidone-2-(oxy)-(1) (DMPOX) adduct in the EPR spectra indicated that other strong oxidizing species may exist [45]. Scavenger experiments were performed. The negligible effect of adding respective methanol (Fig. 6b) and benzoic acid (Figs. 6c and S22) further rules out the involvement of radical species  $\bullet\text{OH}$  and  $\text{SO}_4^{\bullet-}$  [46]. However, adding of the typical trapping agent for singlet oxygen (L-histidine) showed a significant inhibition on the reaction rate with 97.3% degree (Figs. 6b and S23–24) [47,48]. These results indicate that singlet oxygen ( $^1\text{O}_2$ ) may be the main active species involved in the reaction. The detected EPR signal in Fig. 6d with TEMP as the trapping agent further confirmed



**Scheme 1.** Schematic illustration for the engineering of the dual reaction sites on the catalyst - adsorption site for tetracycline (blue background color) and activation site for PDS (red background color).

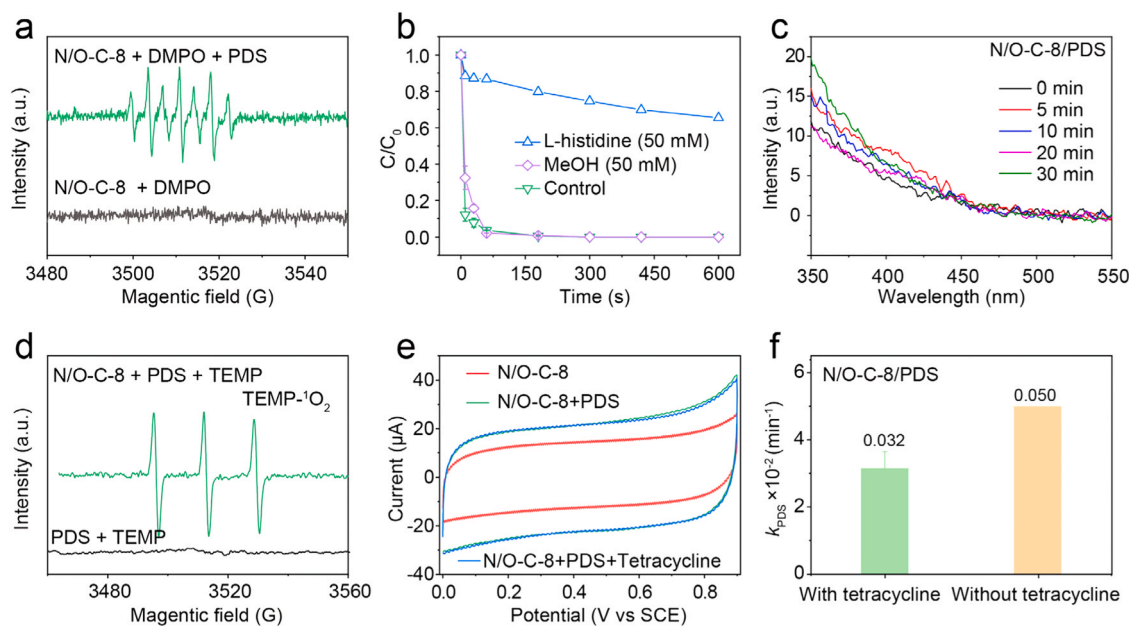


**Fig. 6.** Identification of the active species involved in the catalytic reaction. a) EPR spectra with DMPO as the trapping agent. b) Comparison of reaction rate with different scavengers. c) Detection of hydroxyl radical ( $\bullet\text{OH}$ ) in N/O-C-8/PDS system via benzoic acid oxidation method. The absence of peak  $\sim 412$  nm revealed that there was no detectable hydroxyl radical existed in the reactions. Reaction condition: [benzoic acid] = 10 mg/L, [PDS] = 0.18 mM, [catalyst] = 0.1 g/L, reaction volume = 20 mL, pre-equilibrium 30 min before reaction. d) EPR spectra with TEMP as the trapping agent. e) CV curves measurement under different situations. f) The PDS decomposition rate under catalysis of N/O-C-8, with and without the presence of tetracycline.

the presence of  $^1\text{O}_2$  [49]. Additionally, we excluded the electron transfer mechanism by the electrochemical experiment in Fig. 6e, since the addition of tetracycline didn't cause any change to the detected current [50]. Thus, it can be concluded that  $^1\text{O}_2$  is the main active species responsible for the degradation reaction. It should be pointed out that, activation of PDS becomes slower with the presence of tetracycline in solution, than without tetracycline (Fig. 6f and S25–26). The slightly inhibition effect of tetracycline to PDS decomposition may be possibly brought by the adsorption of tetracycline on the catalyst surface, which spatially disrupted the contact of PDS with the catalyst in some extent. This phenomenon also helps to further evidenced that both the adsorption of tetracycline and activation of PDS are the reaction happened on catalyst surface.

Additionally, we measured the removal performance of catalyst N/O-C-8 toward tetracycline with low concentration (1  $\mu\text{g/L}$ ) contained in drinking water (please refer to Table S5 for the water parameter measurement). As shown in Fig. 7a and b, N/O-C-8 presented a fast removal of tetracycline in the low concentration (1  $\mu\text{g/L}$ ), with an over 90% adsorption contribution. We further applied the catalyst to treat another two representative emerging contaminants bisphenol A and 2,4-dichlorophenol, which were both efficiently removed (Fig. 7a and b, Fig. S27 and Fig. S28). The fast removal of tetracycline in both high and low concentration, as well as bisphenol A and 2,4-dichlorophenol may suggest the application of this catalyst for the broader use for different organic contaminants. The catalytic performance of N/O-C-8 against pH variation was investigated next. As shown in Fig. 7c, the degradation of tetracycline with the catalyst/PDS system remained stable in pH from 2 to 9, indicating a wide working pH range. Moreover, the catalyst shows a stable degradation of tetracycline in the existence of natural organic matter (NOM, such as humic acid) and anions ( $\text{Cl}^-$ ,  $\text{F}^-$ ,  $\text{SO}_4^{2-}$  and  $\text{NO}_3^-$ ), further revealing its great potential for remediation of actual water bodies (Fig. 7d, S29 and S30). The degradation products of tetracycline were analyzed via UHPLC-MS (Fig. S31). The intermediates detected at reaction time of 5 mins (compound B,  $m/z$  461, and compound C,  $m/z$  477) were reported as toxic compounds to fish, daphnid and algae in aquatic environment [49]. However, after the reaction time was extended to 30 mins, the two intermediates were thoroughly

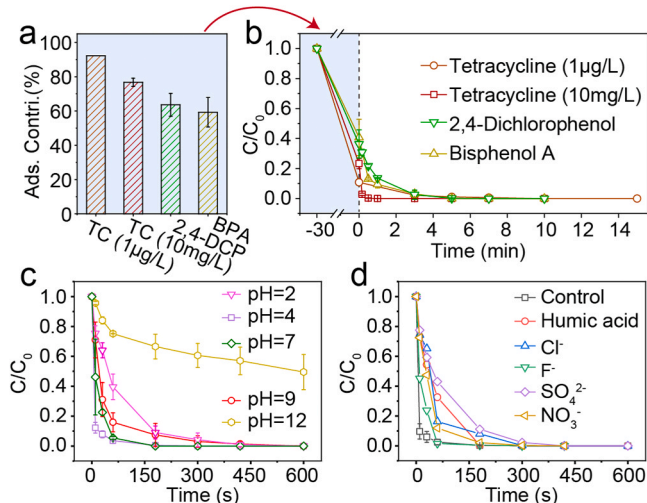


**Fig. 7.** Investigation of the catalyst for practical application. a) The adsorption removal performance of the catalyst in two concentrations (10 mg/L and 1  $\mu\text{g/L}$ ), 2,4-dichlorophenol and bisphenol A, respectively. b) The overall removal performance of the corresponding organic pollutant systems in a). c) The degradation performance of tetracycline in solutions under different pH values. d) The degradation performance of tetracycline in solutions with the presence of different anions and humic acid. Reaction condition if required: [tetracycline] = 10 mg/L or 1  $\mu\text{g/L}$ , [2,4-dichlorophenol] = [bisphenol A] = 10 mg/L, [PDS] = 0.18 mM, [N/O-C-8] = 0.1 g/L, reaction volume = 20 mL, humic acid = 10 mg,  $\text{Cl}^- = \text{F}^- = \text{SO}_4^{2-} = \text{NO}_3^- = 10$  mM, pre-equilibrium 30 min before reaction.

destroyed (Fig. S31b). The possible degradation pathway of tetracycline was proposed and presented in Fig. S32.

We set up a continuous flow experiment as shown in Fig. 8a. Composite N/O-C-8 was placed in the middle of a syringe, while the both side of the syringe was blocked with polyurethane foam to prevent the leakage of catalyst. The tetracycline solution flowed through the syringe

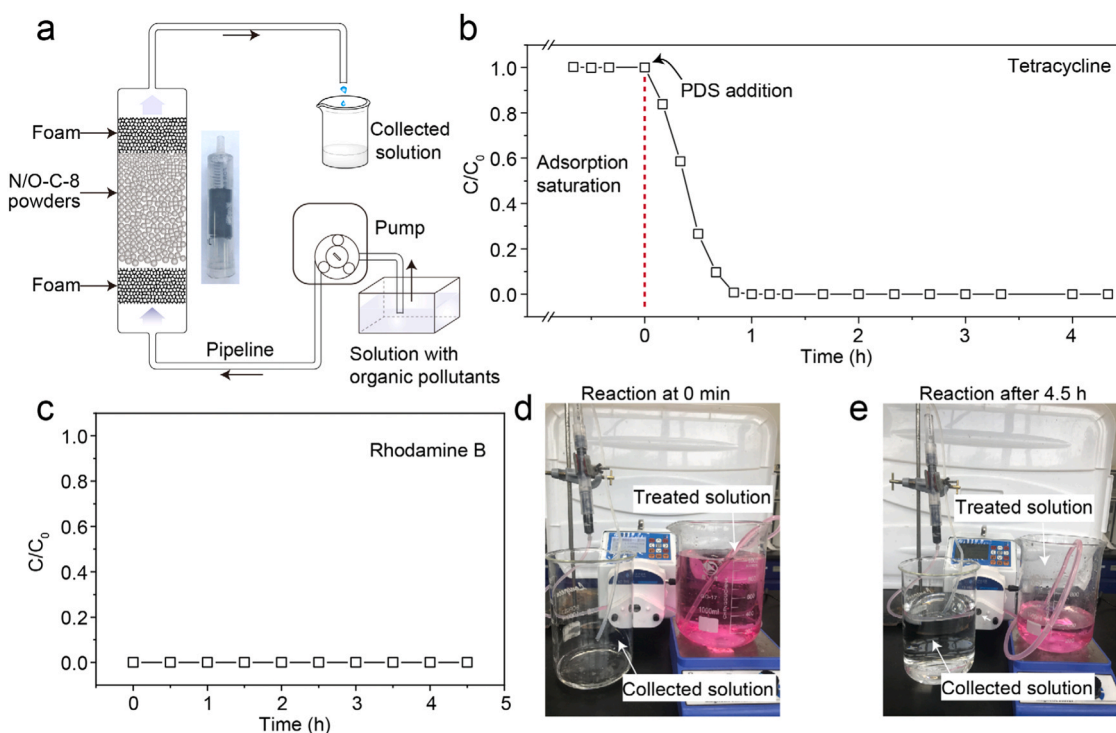


**Fig. 8.** The continuous flow experiment for removal of tetracycline and rhodamine B. a) Schematic illustration of the experiment set; b) The removal performance of tetracycline by the continuous flow set; c) The removal of rhodamine B by the continuous flow set; d and e) Digital photo of the working set before and after the treatment of rhodamine B. Reaction condition: [N/O-C-8] = 40 mg, [PDS] = 1 mM, [tetracycline] = 10 mg/L in tap water (if required), [rhodamine B] = 5 mg/L in tap water (if required), flow rate = 4 mL/min.

with a flow rate of 4 mL/min and collected at the other end. As shown in Fig. 8b, after the physical adsorption of tetracycline saturated, PDS was added into the solution. With the addition of PDS, the tetracycline concentration decreased quickly and reached around zero within 0.5 h. During the next 4 h, the system presented a stable efficient degradation of tetracycline. This experiment not only show the promising catalysis performance of the N/O-C-8/PDS system, but also evidenced that this is an adsorption-assisted catalytic degradation of target molecule, instead of simple physical adsorption. We also use rhodamine B as the target molecule in the continuous experiment (Fig. 8c-e). During a continuous 4.5 h experiment, the collected solution presents colorless, proving the efficient degradation of rhodamine B.

#### 4. Conclusions

Overall, we fabricated a N/O-codoped carbon based catalyst through a pyrolysis technique. With EDTA and DCD as the respective oxygen and nitrogen sources, the as-fabricated catalyst was designed with sufficient content of pyridinic N and carbonyl groups, which were elucidated as adsorption site of target organic molecule and activation site for PDS, respectively. Singlet oxygen was identified as the activation production of PDS, for the degradation of tetracycline. Since both  $^1\text{O}_2$  and tetracycline are located near the catalyst surface,  $^1\text{O}_2$  can reach and oxidize the target molecule tetracycline quickly and efficiently. Additionally, the  $^1\text{O}_2$ -based Fenton-like reaction presented excellent removal efficiency towards more organic pollutants including bisphenol A and 2,4-dichlorophenol, and showed high tolerance to pH variation (pH 2–9), as well as the presence of natural organic matter (humic acid) and anions ( $\text{Cl}^-$ ,  $\text{F}^-$  and  $\text{NO}_3^-$ ), indicating its great potential for practical wastewater treatment. Herein, the pyridinic N/carbonyl group-surface riched composite presented a cost-effective catalyst which may not only applied for practical water remediation, but may also inspire the development of efficient catalysts for other redox reactions.

#### CRediT authorship contribution statement

S. Z. Investigation, Methodology, Writing- original draft. S. Z. Software, Computation. J. W. and W. L. Investigation. J. W. Conceptualization, Supervision, Funding acquisition, Writing-review & editing.

#### Declaration of Competing Interest

The authors declare that they have no known competing financial interests or personal relationships that could have appeared to influence the work reported in this paper.

#### Acknowledgements

We thank the funding support provided by National Natural Science Foundation of China (No. 22176170, 21976152) and the Outstanding Youth Project of Zhejiang Natural Science Foundation, China (No. LR21B070002).

#### Appendix A. Supporting information

Supplementary data associated with this article can be found in the online version at [doi:10.1016/j.apcatb.2021.120783](https://doi.org/10.1016/j.apcatb.2021.120783).

#### References

- [1] B.C. Hodges, E.L. Cates, J.H. Kim, Challenges and prospects of advanced oxidation water treatment processes using catalytic nanomaterials, *Nat. Nanotechnol.* 13 (2018) 642–650. (<https://www.nature.com/articles/s41565-018-0216-x>).
- [2] D.B. Miklos, C. Remy, M. Jekel, K.G. Linden, J.E. Drewes, U. Hubner, Evaluation of advanced oxidation processes for water and wastewater treatment - a critical review, *Water Res.* 139 (2018) 118–131, <https://doi.org/10.1016/j.watres.2018.03.042>.
- [3] E. Neyens, J. Baeyens, A review of classic Fenton's peroxidation as an advanced oxidation technique, *J. Hazard. Mater.* 98 (2003) 33–50, [https://doi.org/10.1016/S0304-3894\(02\)00282-0](https://doi.org/10.1016/S0304-3894(02)00282-0).



- [46] J. Zhou, X.Q. An, Q.W. Tang, H.C. Lan, Q. Chen, H.J. Liu, J.H. Qu, Dual channel construction of WO<sub>3</sub> photocatalysts by solution plasma for the persulfate-enhanced photodegradation of bisphenol A, *Appl. Catal. B: Environ.* 277 (2020), 119221, <https://doi.org/10.1016/j.apcatb.2020.119221>.
- [47] Y.P. Guo, Z.Q. Zeng, Y.C. Zhu, Z.G. Huang, Y. Cui, J.Y. Yang, Catalytic oxidation of aqueous organic contaminants by persulfate activated with sulfur-doped hierarchically porous carbon derived from thiophene, *Appl. Catal. B: Environ.* 220 (2018) 635–644, <https://doi.org/10.1016/j.apcatb.2017.08.073>.
- [48] S.L. Nimai, H. Zhang, Z.L. Wu, N.W. Li, B. Lai, Efficient degradation of sulfamethoxazole by acetylene black activated peroxydisulfate, *Chin. Chem. Lett.* 31 (2020) 2657–2660, <https://doi.org/10.1016/j.ccllet.2020.08.008>.
- [49] L.J. Bu, J. Ding, N.Y. Zhu, M.H. Kong, Y.T. Wu, Z. Shi, S.Q. Zhou, D.D. Dionysiou, Unraveling different mechanisms of persulfate activation by graphite felt anode and cathode to destruct contaminants of emerging concern, *Appl. Catal. B: Environ.* 253 (2019) 140–148, <https://doi.org/10.1016/j.apcatb.2019.04.030>.
- [50] R.L. Yin, W.Q. Guo, N.Q. Ren, L.X. Zeng, M.S. Zhu, New insight into the substituents affecting the peroxydisulfate nonradical oxidation of sulfonamides in water, *Water Res.* 171 (2020), 115374, <https://doi.org/10.1016/j.watres.2019.115374>.